Chemical Physics 84 (1984) 295–309
North-Holland, Amsterdam

A DISSOCIATIVE ELECTROIONIZATION STUDY OF NITROUS OXIDE. THE O^+ AND N^+ DISSOCIATION CHANNELS

J.L. OLIVIER, R. LOCHT and J. MOMIGNY

Institut de Chimie, Département de Chimie Générale et Chimie Physique, Université de Liège, Sart Tilman par B-4000 Liège I, Belgium

Received 25 May 1983; in final form 10 October 1983

After the investigation of the decay of N_2O into NO^+ and N_2^+, the dissociation channels leading to O^+ and N^+ are examined by electroionization using ion kinetic energy and mass analysis. Appearance energies of O^+ and N^+ are measured as a function of the kinetic energy of the fragment ions. Predissociation is the main mechanism for ion production in both channels. In the O^+ decay channel, the $^4\Sigma^-$ state is an important intermediate. The neutral $N_2(X\,^1\Sigma_g^+)$ mainly appears vibrationally excited. In the N^+ dissociation channel, $^2\Pi$ states have to play an important role by predissociating the $N_2O^+(\tilde{C}\,^2\Sigma^+)$ state and the higher-lying doubly excited states of N_2O^+.

1. Introduction

In our earlier work [1] we analyzed the dissociation of N_2O leading to NO^+ and N_2^+ under the impact of electrons from 10 to 40 eV impinging energy. For both ions the kinetic energy distributions were examined as a function of the electron energy and the kinetic energy versus appearance energy diagrams were discussed.

In the present paper the two other dissociative ionization channels of nitrous oxide, producing respectively N^+ and O^+, will be studied in the same way. Whereas the O^+ ion has been studied by photoionization [2] and photoion–photoelectron coincidence techniques [3–5], the former ion N^+ could only be observed in the threshold region [2].

2. Experimental

The experimental arrangement used in the present work has been described in detail earlier [6] and only the prominent features will be repeated here. The ions generated in a Nier-type ion source by the impact of energy-controlled electrons, are focused on the exit hole, energy analyzed by a retarding lens and mass selected in a quadrupole mass filter. The ion current, collected on a Cu–Be electron multiplier, is continuously measured as a function of either the electron energy at fixed retarding potential or the retarding potential at fixed electron energy. Both signals are electronically differentiated, averaged in a multichannel analyzer which is interfaced with a Tracor TN-4000 minicomputer. The data are stored on floppy-disk for further handling and recording.

The operating conditions maintained during this work are identical to those described previously [1].

The maximum of the N_2O^+ ion energy distribution is used as the zero-energy calibration point for the ion kinetic energy scale. The same reference is used when the ionization efficiency curves of O^+ and N^+ are recorded at different retarding potential settings.

The first adiabatic ionization energy of N_2O, i.e. 12.886 eV [2], is used to calibrate the ionizing electron energy scale. The electron energies indicated for all the ion kinetic energy distributions presented in this work, are corrected with respect to the same standard.

All the threshold energy measurements were independently repeated at least five times and the

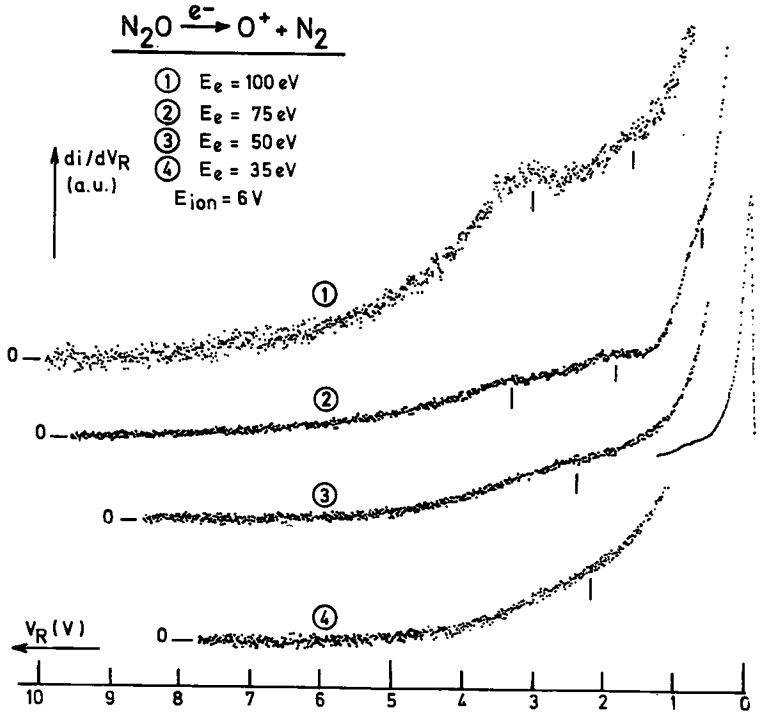

Fig. 1. First derivative of the retarding potential (V_R) curves of O^+ at 35–100 eV impinging electron energies.

appearance energies quoted here are averaged values. The errors are given by the standard deviation σ. In the kinetic energy versus appearance energy diagrams, linear regressions are used to fit the experimental data.

The ion kinetic energy spectra were recorded thirty to fourty times for low electron energies, i.e. 15–25 eV. The ion kinetic energy values listed below are the average position of submaxima and the quoted error is given by the standard deviation σ.

3. Results

3.1. The O^+ ions

The ion energy distribution. The O^+ ion energy distribution spectra, recorded at high electron energies, are reproduced in fig. 1. At all electron energies, the main peak is at thermal energy. At 100 and 75 eV, less intense shoulders are observed around 0.6, 1.6 and 3.2 eV. Below 50 eV electron

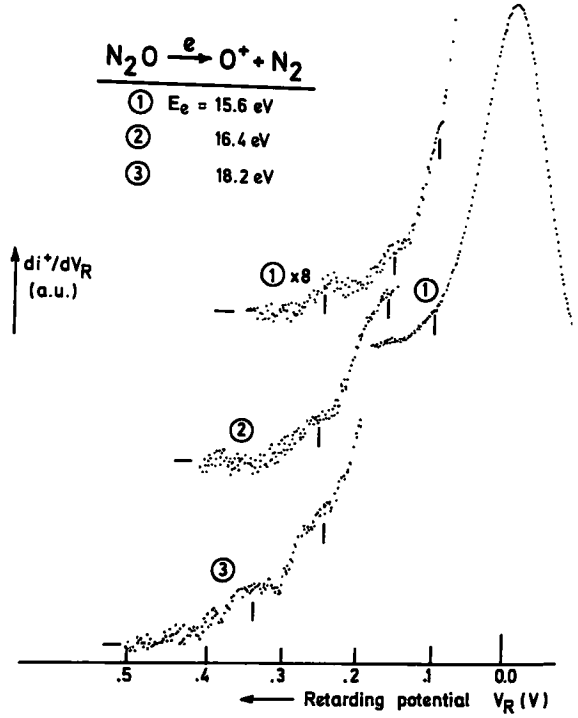

Fig. 2. Kinetic energy distribution of O^+ near threshold.

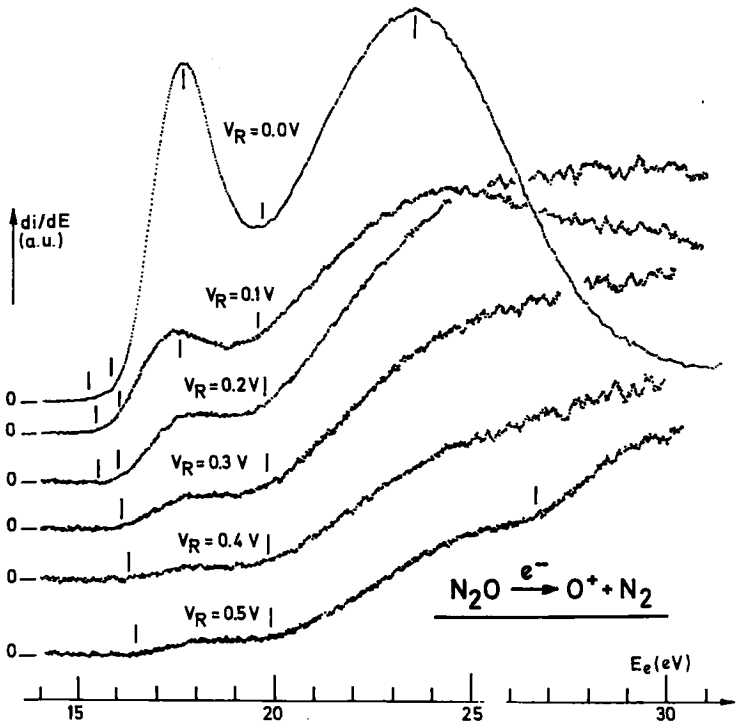

Fig. 3. First derivative of the ionization efficiency curves of O^+ at retarding potential settings V_R = 0.0–0.5 eV.

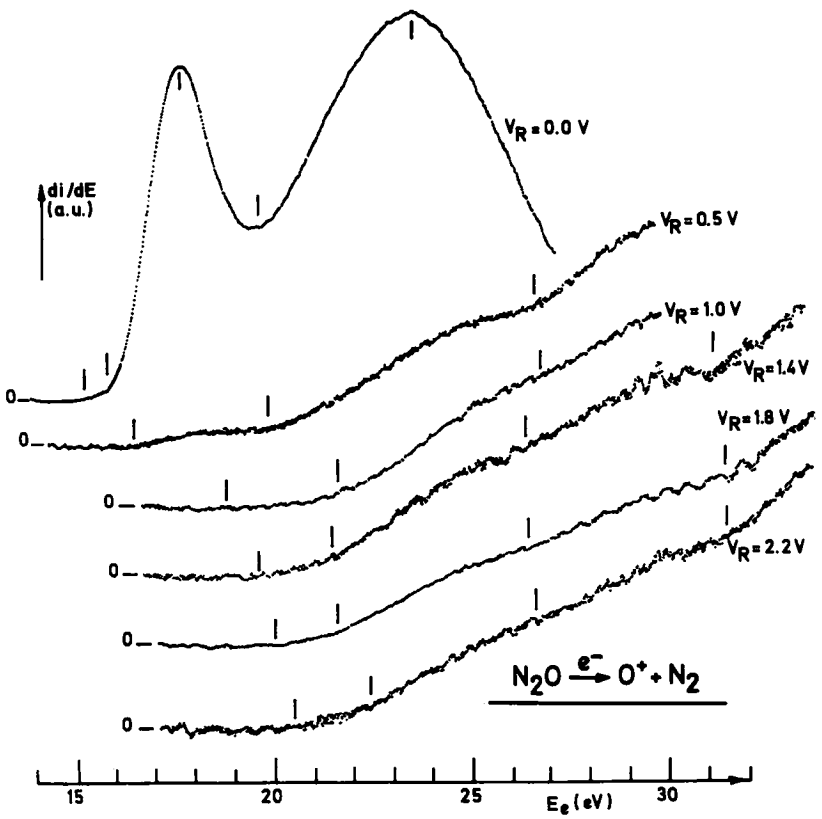

Fig. 4. First derivative of the ionization efficiency curves of O^+ at retarding potential settings V_R = 0.0–2.2 V.

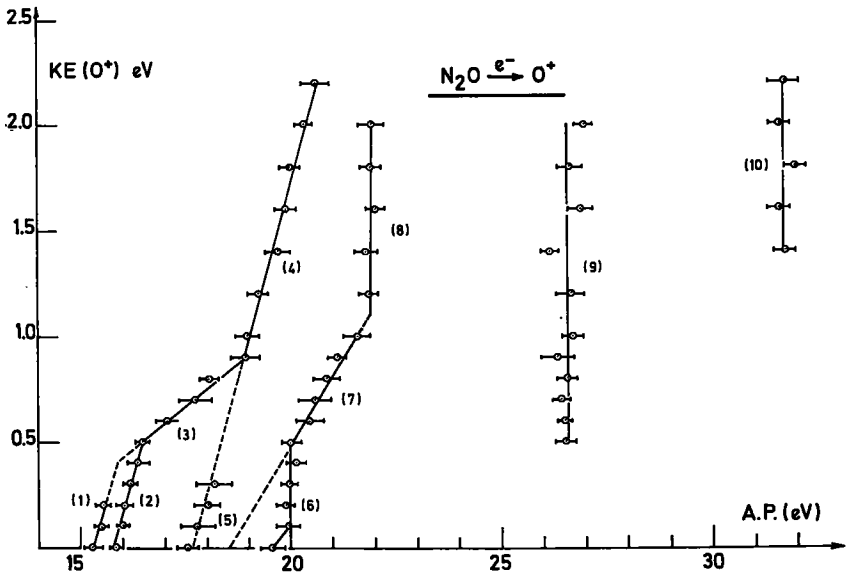

Fig. 5. Kinetic energy versus appearance energy diagram for O^+/N_2O.

energy a shoulder is observed around 2.2 eV.

In the threshold region, i.e. in the electron energy range of 18–15.4 eV, the distribution is modulated by weak maxima as shown in fig. 2. These structures are measured at 102 ± 10, 148 ± 15 and 239 ± 15 meV. At 18 eV electron energy a maximum at 320 ± 20 meV becomes visible.

The ionization efficiency curves. A set of first derivative of the ionization efficiency curves of O^+ from N_2O, as recorded at different retarding potential settings V_R, is shown in figs. 3 and 4. The shape of these changes dramatically for low retarding potential settings, i.e. 0.0–0.5 eV (see fig. 3), whereas it remains quite constant over the range of 0.6 to 2.5 eV retarding potential (see fig. 4).

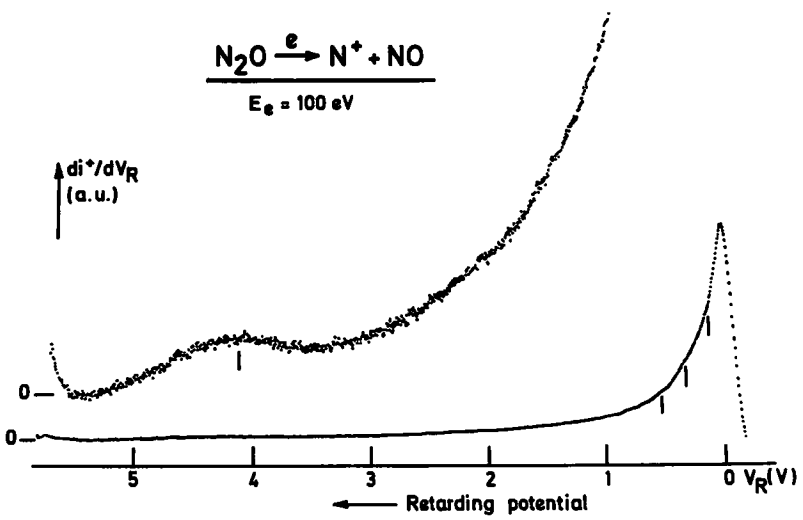

Fig. 6. Kinetic energy distribution of N^+ at 100 eV electron energy.

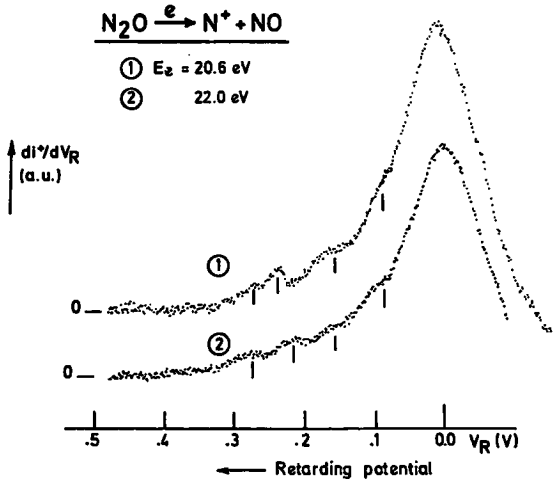

Fig. 7. Kinetic energy distribution of N^+ near threshold.

Several onsets are measured respectively at 15.27 ± 0.18, 15.83 ± 0.17 and 19.56 ± 0.3 eV. Two maxima are observed at 17.53 ± 0.25 and ≈ 23.4 eV. The kinetic energy versus appearance energy plot is shown in fig. 5.

3.2. The N^+ ions

The ion energy distribution. The N^+ ion kinetic energy distribution recorded at high electron energies is dominated by a thermal peak broadened toward high ion energies (see fig. 6). The weak maximum observed around 4.1 eV disappears at 50 eV electron energy. For electron energies close to the onset of N^+, i.e. at 20.6–22.0 eV, the ion energy distribution clearly shows structures measured at 79 ± 7, 155 ± 15 and 256 ± 15 meV (see fig. 7).

The ionization efficiency curves. First derivative of the ionization efficiency curves of N^+, as recorded at different retarding potential settings, are reproduced in fig. 8. Appearence energies of N^+ are measured at 20.26 ± 0.15, 21.16 ± 0.23, 27.65 ± 0.5, 31.9 ± 0.3 and 39.1 ± 0.2 eV. The kinetic energy versus appearance energy plot is shown in fig. 9.

4. Discussion

For both dissociation channels, leading to O^+ and N^+ respectively, we will discuss separately

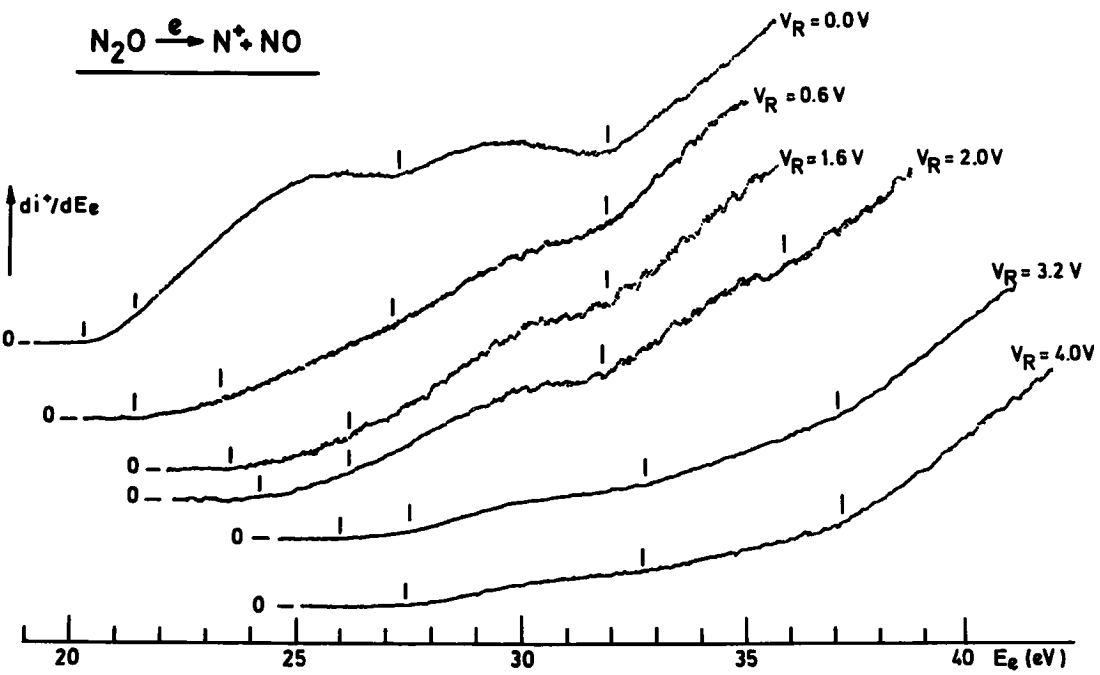

Fig. 8. First derivative of the ionization efficiency curves of N^+ at retarding potential settings $V_R = 0$–4.0 V.

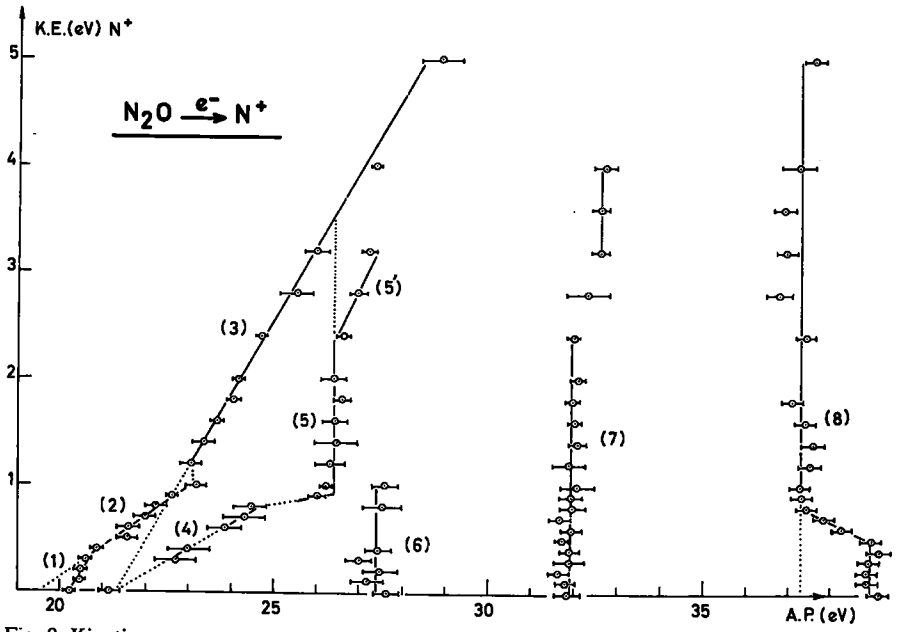

Fig. 9. Kinetic energy versus appearance energy diagram for N^+/N_2O.

each portion of the corresponding kinetic energy versus appearance energy plots shown in figs. 5 and 9.

Table 1
Products and calculated energies (eV) for the dissociation channels $N_2O+e^- \rightarrow O^+ + N_2$ using $D(N_2-O)=1.677$ eV [7], $D(N_2)=9.756$ eV [8] and IP(OI) = 13.614 eV [9]. For the excitation energies of OI and N_2, see ref. [9] and ref. [8] respectively (1 eV = 8065.73 cm^{-1} [9])

$O^+(^4S)+N_2(X\,^1\Sigma_g^+)$	15.291	(1)
$O^+(^2D)+N_2(X\,^1\Sigma_g^+)$	18.614	(2)
$O^+(^2P)+N_2(X\,^1\Sigma_g^+)$	20.308	(3)
$O^+(^4S)+N_2(A\,^3\Sigma_u^+)$	21.460	(4)
$O^+(^4S)+N_2(B\,^3\Pi_g)$	22.614	(5)
$O^+(^4S)+N_2(B'\,^3\Sigma_u^-)$	23.455	(6)
$O^+(^4S)+N_2(a'\,^1\Sigma_u^-)$	23.839	(7)
$O^+(^2D)+N_2(A\,^3\Sigma_u^+)$	24.783	(8)
$O^+(^4S)+N(^4S)+N(^4S)$	25.047	(9)
$O^+(^2D)+N_2(B\,^3\Pi_g)$	25.967	(10)
$O^+(^2P)+N_2(A\,^3\Sigma_u^+)$	26.477	(11)
$O^+(^4S)+N(^4S)+N(^2D)$	27.430	(12)
$O^+(^2P)+N_2(B\,^3\Pi_g)$	27.661	(13)
$O^+(^2D)+N(^4S)+N(^4S)$	28.370	(14)
$O^+(^4S)+N(^4S)+N(^2P)$	28.623	(15)
$O^+(^4S)+N(^2D)+N(^2D)$	29.813	(16)
$O^+(^2P)+N(^4S)+N(^4S)$	30.064	(17)
$O^+(^4P)+N_2(X\,^1\Sigma_g^+)$	30.149	(18)
$O^+(^2D)+N(^4S)+N(^2D)$	30.753	(19)
$O^+(^4S)+N(^2D)+N(^2P)$	31.006	(20)

4.1. The O^+ dissociation channel

The calculated energy and products for different dissociation limits between 15 and 31 eV are listed in table 1 by increasing energy.

The first onset of O^+ has been measured at 15.27 ± 0.18 eV and is in good agreement with the photoionization value, i.e. 15.25 eV [2] and the thermochemical value calculated for process (1) in table 1.

The first straight line starting at 15.27 eV (see fig. 5) is defined by only three experimental points extending from 0 to 0.2 eV kinetic energy. The slope is ≈ 0.73. This value corresponds fairly well with the slope given by the ratio $m_{N_2}/m_{N_2O} = 0.64$ when no internal energy is involved in the dissociation. The excess energy with respect to 15.27 eV is thus entirely converted into translational energy. As shown in fig. 2, part of the O^+ ions appearing in the threshold region carry only thermal energy. A weak structure is observed at higher retarding potentials, i.e. higher ion energies.

As for NO^+ [1], the appearance energy of O^+ lies in the energy range of the potential well of the $N_2O^+(\tilde{X}\,^2\Pi)$ state. Furthermore, it is known from photoelectron spectroscopy [10] that the ground

Table 2
Discrete values (meV) observed in the kinetic energy distribution of O^+/N_2O. Column 3 is the total energy calculated with respect to the O^+ onset energy

KE (O^+)	Total KE	Total energy (eV)	Autoionization [2]
0.0	0.0	15.27±0.18	15.250
102±10	160±15	15.43±0.20	15.431 (3dσ)
148±15	232±23	15.50±0.20	15.532 (4dπ)
239±15	375±23	15.64±0.20	15.671 (5pσ)
320±20	503±30	15.77±0.21	15.791 (5dσ)

state of N_2O^+ is populated between 12.88 and 13.4 eV by direct Franck–Condon transitions. The photoionization efficiency curve of N_2O^+ shows abundant autoionization structure between the ionization onset of N_2O^+ and 16.39 eV [2,10].

The fine structure observed in the kinetic energy distribution is usually correlated with predissociation [11]. In terms of total kinetic energy, the discrete values of the kinetic energy are listed in table 2 and related to the autoionization structure in the photoionization efficiency curve [2]. Good agreement is observed between the present measurements and the prominent features in the photoionization efficiency curve.

To account for the present experimental results, the O^+ ions have to be produced by a two-step mechanism

$$N_2O + e^- \rightarrow N_2O^* + e^-,$$

$$N_2O^* \rightarrow N_2O^+(\tilde{X}\,^2\Pi, v^*) + e^-$$

$$\xrightarrow[^4\Sigma^-]{\text{pred.}} N_2\left(X\,^1\Sigma_g^+, v=0\right) + O^+(^4S) + KE,$$

where the $N_2O^+(\tilde{X}\,^2\Pi)$ state is first produced into highly excited vibrational levels through autoionization, as it turns out from threshold photoelectron–photoion coincidence experiments [4,5].

Furthermore, the combination of the spectroscopic terms ^4S and $^1\Sigma_g^+$ gives rise to only one molecular state in the linear configuration of N_2O^+, i.e. a $^4\Sigma^-$ state. Lorquet and Cadet [12] calculated this state to be repulsive, and predissociating the $\tilde{X}\,^2\Pi$ state.

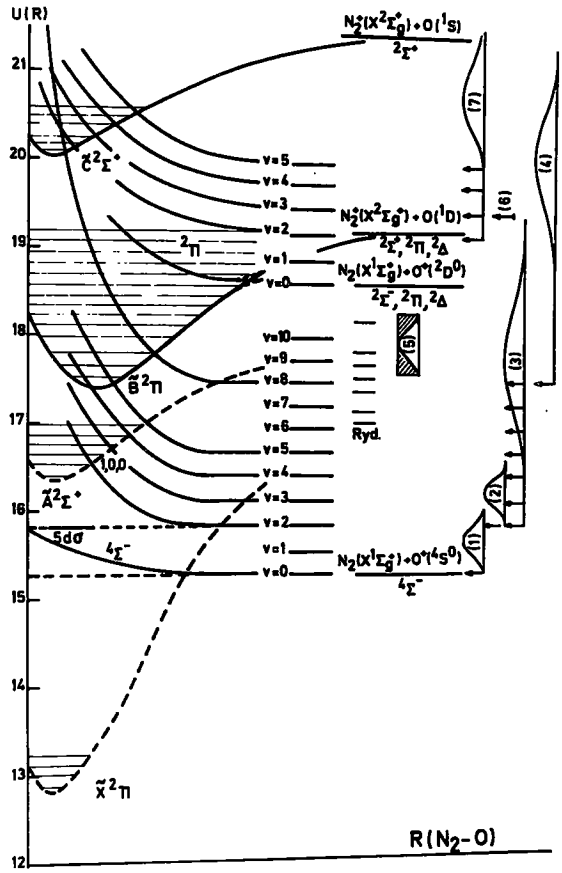

Fig. 10. Schematic potential energy diagram of N_2O along the N_2–O^+ coordinate. For explanation of the different parts, see text.

The interpretation of the present results agrees with that of the photoionization experiments [2,4,5] which show the existence of Rydberg series converging to the $\tilde{A}\,^2\Sigma^+$ state of N_2O^+. The coincidence work [5] evidenced O^+ ion formation by dissociative autoionization and predissociation of high vibrationally excited $N_2O^+(\tilde{X}\,^2\Pi)$ levels.

The above discussed mechanism is illustrated by a schematic drawing of a two-dimensional potential energy diagram (see fig. 10).

A second onset, measured at 15.83 ± 0.17 eV is observed in the first derivative of the ionization efficiency curve of O^+ by a steep rise of the signal. This group of ions is observed over a wide ion kinetic energy range, i.e. 0–2.5 eV. Several processes and dissociation limits have to be in-

voked to account for these results.

Segment (2) in the diagram shown in fig. 5 extends from 0 to 0.5 eV and is defined by six onsets between 15.83 and 16.48 eV. A least-squares fit of these points gives a straight line with a slope of 0.73 and an extrapolated onset energy $AP(O^+)$ of 15.80 eV for $KE(O^+) = 0$ eV with a correlation coefficient $r = 0.983$.

A look at the onset energies listed in table 1 clearly shows that the threshold at 15.83 eV lies well below the onset of process (2) which produces the O^+ ion in its first excited state ^2D. The onset at 15.83 eV could consequently only be ascribed to the formation of the N_2 molecule in a vibrational excited state. Taking $\omega_e(N_2, X\,^1\Sigma_g^+) = 2358\ cm^{-1}$ [8], the energy difference of $15.83 - 15.27 = 0.56$ eV fits, within experimental error, two vibrational quanta of the $N_2(X\,^1\Sigma_g^+)$ molecule.

A comparison of the slope of 0.64, obtained by considering the excess energy with respect to 15.83 eV entirely converted into translational energy, and the experimental slope of 0.73, would point out that no further internal energy is involved. The only mechanism which could account for the onsets from 15.83 to 16.48 eV is

$$N_2O + e^- \rightarrow N_2O^* + e^-,$$

$$N_2O^* \rightarrow N_2O^+(\tilde{X}\,^2\Pi) + e^-$$

$$\xrightarrow[^4\Sigma^-]{\text{pred.}} N_2\left(X\,^1\Sigma_g^+, v = 2\right) + O^+(^4S) + KE,$$

where the upper vibrational levels of $N_2O^+(\tilde{X}\,^2\Pi)$, populated by autoionization, are predissociated by the $^4\Sigma^-$ state (see fig. 10). It is worth noting that an intense autoionization peak is observed at 15.84 eV in the photoionisation efficiency curve of O^+ [2].

The $v = 0, 0, 0$ level of the $\tilde{A}\,^2\Sigma^+$ state of N_2O^+ being at 16.388 eV [10], in the energy range considered here, it is not predissociated for the following reasons: (i) its fluorescence quantum yield is 1.0 ± 0.3 [13] and (ii) no coincidence is measured between O^+ photoions and photoelectrons corresponding to the ionization of N_2O^+ in the $\tilde{A}\,^2\Sigma^+$, $v = 0, 0, 0$ state [3]. As a result, this level can be discarded as an intermediate in the energy range 15.83–16.48 eV.

A sudden break is observed in the kinetic energy versus appearance energy diagram (see fig. 5) at 16.48 eV. The straight line labelled (3) extends from 16.48 to 19.00 eV with a slope of 0.16. Compared to the expected slope of 0.64, the experimental slope indicates the conversion of 75% of the excess energy with respect to 15.27 eV into internal energy of the $X\,^1\Sigma_g^+$ state of the N_2 molecule. An energy balance made on each experimental threshold measurement in the O^+ ion kinetic energy range 0.5–0.9 eV, shows the $N_2(X\,^1\Sigma_g^+)$ molecule to be formed in the vibrational levels $v = 2$–8.

The position in energy of the break, i.e. 16.48 eV corresponds fairly well to the ionization energy of the $\tilde{A}\,^2\Sigma^+$, $v = 1, 0, 0$ state of N_2O^+. By photoelectron spectroscopy this energy is measured at 16.56 eV [10]. The $N_2O^+(\tilde{B}\,^2\Pi)$ state lies at 17.65 eV [10] and the photoelectron band corresponding to this state extends up to 19.2 eV.

The interpretation of the O^+ ion formation in this energy range would be

$$N_2O + e^- \rightarrow N_2O^+(\tilde{A}\,^2\Sigma^+ \text{ and } \tilde{B}\,^2\Pi) + 2e^-$$

$$\xrightarrow[^4\Sigma^-]{\text{pred.}} N_2\left(X\,^1\Sigma_g^+, v = 2\text{–}8\right) + O^+(^4S),$$

where both the $\tilde{A}\,^2\Sigma^+$ and the $\tilde{B}\,^2\Pi$ states of N_2O^+ are predissociated almost completely by the $^4\Sigma^-$ state (see fig. 10). No discontinuity is observed between 17.0 and 17.6 eV corresponding to the Franck–Condon gap between the $\tilde{A}\,^2\Sigma^+$ and the $\tilde{B}\,^2\Pi$ states. The population of Rydberg series converging to the $N_2O^+(\tilde{B}\,^2\Pi)$ state has to be invoked. Higher vibrational levels of the $\tilde{A}\,^2\Sigma^+$ state could be populated through autoionization and subsequently undergo predissociation.

The present experimental results confirm the photoionization [2] and photoion–photoelectron coincidence [3–5] experiments. The latter shows the $\tilde{A}\,^2\Sigma^+$ and $\tilde{B}\,^2\Pi$ states to be predissociated in the O^+ producing channel. The photoionization experiment clearly shows the importance of autoionization in the same energy range.

Recent ab initio quantum-mechanical calculations [14] showed that within the energy range of the $\tilde{B}\,^2\Pi$ state, i.e. 17.6–19.2 eV, two ionic states

with almost equal spectral intensities, interact vibrationally through both totally symmetric modes. It is not excluded that these states are both involved in this energy range.

A second drastic change in slope occurs at 19.0 eV and a straight line extends up to 20.67 eV with a slope of 0.72 and extrapolates to 17.65 eV for $KE(O^+) = 0$ eV. This segment denoted (4) in fig. 5 covers a kinetic energy range of 0.9 to 2.0 eV.

The correspondence between the experimental slope, and that expected for total conversion of the excess energy into translational energy, means that over the energy range considered the dissociation products remain in the same vibronic state. The extrapolated value of 17.65 eV is still too low to ascribe this energy to the appearance of N_2 and/or O^+ in an electronically excited state through e.g. process (2) in table 1. The energy of 17.65 eV is only compatible with a mechanism allowing the formation of $N_2(X\,^1\Sigma_g^+)$ in its vibrational level $v = 8$ accounting for the energy difference 17.65 − 15.27 = 2.38 eV and producing O^+ fragments with at least 0.9 eV kinetic energy.

Below the ionization potential of the $N_2O^+(\tilde{C}\,^2\Sigma^+)$ state, i.e. 20.105 eV [2], the O^+ ions should be produced by dissociative autoionization. The photoionization efficiency curves of both the N_2O^+ and O^+ ions show autoionization peaks corresponding to Rydberg series converging to the $\tilde{C}\,^2\Sigma^+$ state [2]. At these energies, the O^+ producing mechanism would be

$$N_2O + e^- \rightarrow N_2O^* + e^-,$$

$$N_2O^* \xrightarrow[{}^4\Sigma^-]{\text{autoion.}} N_2\left(X\,^1\Sigma_g^+, v = 8\right) + O^+(^4S) + KE,$$

where the Rydberg states autoionize to the $^4\Sigma^-$ state which dissociates. At 20.105 eV and higher electron energies the O^+ appearance mechanism is

$$N_2O + e^- \rightarrow N_2O^+(\tilde{C}\,^2\Sigma^+) + 2e^- \xrightarrow[{}^4\Sigma^-]{\text{pred.}} N_2\left(X\,^1\Sigma_g^+, v = 8\right) + O^+(^4S) + KE.$$

In both processes the total excess energy with respect to the 17.65 eV limit is converted only into translational energy of the fragments.

Zero-energy O^+ ions are observed at 17.65 eV and correspond to the maximum of the first peak observed in the first derivative of the ionization efficiency curve (see fig. 3). The energy shift of the maximum as a function of the O^+ ion kinetic energy is drawn in fig. 5 by a straight line (5). The measurements fit fairly well the extended straight line (4) which has a slope of 0.72. The shift is measurable over the range 17.53 ± 0.25 to 18.2 ± 0.4 eV.

By photoelectron spectroscopy, the $N_2O^+(\tilde{B}\,^2\Pi)$ band covers the energy range 17.6–19.2 eV [10]. Its maximum is at 18.2 eV. The photoionization efficiency curve of O^+ [2] displays autoionization structure in the energy range 743–695 Å (i.e. 16.68–17.84 eV) "with spacings suggesting a vibrational series" [2]. This series should correspond to the first Rydberg component converging to the $\tilde{B}\,^2\Pi$ state.

To interpret this part of the diagram shown in fig. 5 a two-step mechanism has to be invoked, i.e.

$$N_2O + e^- \rightarrow N_2O^*(\text{Rydb.}) + e^-,$$

$$N_2O^*(\text{Rydb.}) \rightarrow N_2O^+(\tilde{B}\,^2\Pi) \xrightarrow[{}^4\Sigma^-]{\text{pred.}} N_2\left(\tilde{X}\,^1\Sigma_g^+, v = 8\right) + O^+(^4S),$$

where the Rydberg state(s) autoionize(s) to the $\tilde{B}\,^2\Pi$ state. This process is inserted in the potential energy diagram of fig. 10.

The threshold at 19.5 ± 0.3 eV corresponds to the onset of the second broad peak in the first derivative of the ionization efficiency curve of the O^+ ion (see fig. 3). The vertical segment (6) in fig. 5, resulting from 25 measurements, occurs at 20.0 ± 0.1 eV. This line is vertical due to the fact that for the onset at 20 eV no energy shift is measured as long as the retarding potential is lower than or equal to the minimum kinetic energy carried by the ions produced at the energy considered.

However the onset at 19.5 ± 0.3 eV, would correspond to O^+ ions with thermal energy. The energy content of N_2O^+ is sufficient to produce process (2) in table 1 where O^+ is formed in its $^2D^\circ$ level. Since the ions carry no kinetic energy, the energy difference of 19.5 − 18.6 = 0.9 eV is to be ascribed to the vibrational energy content of

$N_2(X\,^1\Sigma_g^+)$ species, i.e. $v = 3$. Several mechanisms could lead to these products: (i) The population of the repulsive part of the $^2\Pi$ state calculated by Lorquet and Cadet [12] which converges to the limit at 18.6 eV. (ii) The production of N_2O^+ in the doubly orthogonal state lying at 19.5 eV [15] which could be predissociated by the $^2\Pi$ state. In the same energy range, i.e. 19.25 ± 0.15 eV, the formation of NO^+ ions has been evidenced [1]. The same state would decompose in both channels, $NO^+(X\,^1\Sigma^+, v = 4) + N(^4S)$ and $N_2(X\,^1\Sigma_g^+, v = 3) + O^+(^2D^\circ)$. (iii) The excitation of N_2O in Rydberg states, members of series converging to the $N_2O^+(\tilde{C}\,^2\Sigma^+)$ state. They could autoionize to the $^2\Pi$ state which dissociates at 19.5 eV. The photoionization efficiency curve of O^+ displays autoionization structures in this energy range [2].

In the energy range 20.0–21.7 eV the measured onsets fit straight line (7) characterized by a slope of 0.32 and extrapolated to 18.42 eV. The correlation coefficient is $r = 0.986$.

The extrapolated energy of 18.42 is close to the thermodynamical onset calculated for process (2) in table 1, i.e. 18.614 eV. Furthermore the slope of 0.32, instead of the expected value of 0.64, points out the partition of the excess energy with respect 18.42 eV into internal energy (50%) and translational energy (50%) of the products.

The energy of 20.0 ± 0.25 eV corresponds fairly well to the ionization potential of $N_2O^+(\tilde{C}\,^2\Sigma^+)$ state, i.e. 20.105 eV [2]. In the energy range considered here, the O^+ producing channel is opened through the mechanism

$$N_2O + e^- \rightarrow N_2O^+(\tilde{C}\,^2\Sigma^+) + 2e^-$$
$$\xrightarrow[^2\Pi]{\text{pred.}} N_2(X\,^1\Sigma_g^+, v = 2\text{–}5) + O^+(^2D),$$

where the $\tilde{C}\,^2\Sigma^+$ state is completely predissociated to the 18.61 eV dissociation limit through the $^2\Pi$ state. The energy balance made on the measured onset energies shows the $N_2(X\,^1\Sigma_g^+)$ to be vibrationally excited in $v = 2$, 3, 4 and 5.

The $N_2O^+(\tilde{C}\,^2\Sigma^+)$ state is populated up to 20.7 eV by direct Franck–Condon transition. Upper levels of this state could be reached through autoionization. Furthermore doubly excited states of N_2O^+ are located in this energy range. These states could also be predissociated by the $^2\Pi$ state to the 18.61 limit.

From 22 to 32 eV three vertical lines are observed in the kinetic energy versus appearance energy diagram (see fig. 5), i.e. at 22.0 ± 0.2, 26.6 ± 0.2 and 31.7 ± 0.3 eV. The only information available in this energy range is the existence of N_2O^+ states corresponding to "multiple electron transitions" (MET) or doubly excited states. The energies of these states (vertical ionization energies) were determined by several techniques. The energies as well as the assignments are listed in table 3.

The vertical lines (8), (9) and (10) suggest a large amount of minimum kinetic energy to be involved in these processes. The ion signal intensity for retarding potentials higher than 2.5 eV is too low to give measurable first derivative of the ionization efficiency curves in a time span of 72 h. Therefore it has not been possible to determine the dissociation limits involved in these processes.

However for segment (8) we could predict the dissociation products to be $N_2(X\,^1\Sigma_g^+) + O^+(^4S)$ at 15.29 eV and correlated with the $^4\Sigma^-$ state. The second dissociation limit at 18.61 eV, corresponding to the $O^+(^2D^\circ)$ formation, cannot be discarded, an inclined segment starting at 2.5 eV kinetic energy could have a slope of the order of 0.64 eV. The onset energy of these O^+ ions is in good agreement with the "adiabatic" ionization

Table 3
Ionization energies measured by XPS [18], He(II) PES [15] dipole (e, 2e) coincidence spectroscopy [16]. The valence shell configuration of N_2O is $\ldots(4\sigma)^2(5\sigma)^2(6\sigma)^2(1\pi)^4(7\sigma)^2(2\pi)^4$; $^1\Sigma^+$. Assignments are from ref. [17]

XPS	HeII PES	e, 2e	Ionized orbital
–	22.6	23.5 (I)	1π
24.5	24.1	24.5 (II)	1π
28.5	–	28.5 (III)	1π
33.0	33.7	33.0 (IV)	5σ
35.5	–	35.5 (V)	5σ
39.0	37.3	38.0 (VI)	4σ

energy of the first MET band (see table 3)

$$N_2O + e^- \rightarrow N_2O^{+*} + 2e^-$$
$$\xrightarrow{\text{pred.}} N_2(X\,^1\Sigma_g^+) + O^+(^4S \text{ or } ^2D).$$

In the same way, the energies at 26.6 and 31.7 eV correspond to the MET bands having their maximum at 28.5 and 33.0 eV respectively.

4.2. The N^+ dissociation channel

The kinetic energy versus appearance energy diagram belonging to the N^+ dissociation channel is shown in fig. 9. Dissociation products and energies are listed in table 4.

The first onset for N^+ produced by electroionization of N_2O is measured at 20.26 ± 0.15 eV. This energy is higher than the photoionization threshold, i.e. 20.075 eV [2].

The energy of 20.26 eV is the starting point of a segment labeled (1) in fig. 9. This straight line extends from 0 to 0.4 eV kinetic energy with a slope of 0.66 and a correlation of 0.955. The expected slope when total conversion of electronic to translational energy occurs, is 0.682. The agreement between experimental and expected values of the slope allows us to consider only translational energy being involved in the dissociation process.

The lowest-energy dissociation limit producing N^+ ions is calculated at 19.464 eV [see table 4, process (1)]. The energy difference between the observed and thermodynamic onsets, i.e. $20.26 - 19.46 = 0.80$ eV, is only due to ro-vibrational excitation of the diatomic neutral fragment $NO(X\,^2\Pi)$. Taking the frequency $\omega_e(X\,^2\Pi) = 0.236$ eV [8], the $NO(X\,^2\Pi)$ state energy content of 0.8 ± 0.15 eV corresponds to the vibrational level $v = 4$.

The onset of 20.26 ± 0.15 eV lies close to the ionization energy of the $\tilde{C}\,^2\Sigma^+$ state of N_2O^+ which is measured at 20.105 eV [10]. The segment (1) extends up to 20.9 eV, while the $\tilde{C}\,^2\Sigma^+$ photoelectron band covers the energy range 20.1–20.7 eV [10]. From these considerations, the mechanism for the formation of N^+ at 20.26 eV should be

$$N_2O + e^- \rightarrow N_2O^+(\tilde{C}\,^2\Sigma^+) + 2e^-$$
$$\xrightarrow{\text{pred.}} N^+(^3P) + NO(X\,^2\Pi, v = 4),$$

where the $N_2O^+(\tilde{C}\,^2\Sigma^+)$ state is fully predissociated. This mechanism could account for the few structures observed in the kinetic energy distribution of N^+ recorded near its onset energy. In table 5 a tentative interpretation of this structure is given in terms of the $\tilde{C}\,^2\Sigma^+$ state energy levels. It is not possible to decide whether autoionization is present or not.

For the identification of the predissociating state, in the linear configuration of N_2O^+, eight molecular ion states have to be considered and are correlated with ^3P–$^2\Pi$ terms: doublet and quartet Σ^+, Σ^-, Π and Δ states. Considering the electronic predissociation selection rules only the doublet Σ^+, Σ^- and Π states have to be retained [7], where the $\Delta\Lambda = 0, \pm 1$ is the most restrictive. Lorquet and Cadet [12] calculated a $^2\Pi$ state which crosses the $\tilde{B}\,^2\Pi$ and the $\tilde{C}\,^2\Sigma^+$ states of N_2O^+. This state

Table 4
Products and calculated energies (eV) for the dissociation channels $N_2O + e^- \rightarrow NO + N^+$. $D(ON\text{–}N) = 4.930$ eV [7], $D(NO) = 6.507$ eV [8], IP(NI) = 14.534 eV [9]. For excitation energy of NI and NO see ref. [9] and ref. [8] respectively (1 eV = 8065.73 cm^{-1} [9])

$N^+(^3P)+NO(X\,^2\Pi)$	19.464	(1)
$N^+(^1D)+NO(X\,^2\Pi)$	21.364	(2)
$N^+(^1S)+NO(X\,^2\Pi)$	23.516	(3)
$N^+(^3P)+NO(A\,^2\Sigma^+)$	24.914	(4)
$N^+(^3P)+NO(B\,^2\Pi)$	25.157	(5)
$N^+(^5S)+NO(X\,^2\Pi)$	25.312	(6)
$N^+(^3P)+NO(C\,^2\Sigma^+)$	25.929	(7)
$N^+(^3P)+N(^4S)+O(^3P)$	25.971	(8)
$N^+(^3P)+NO(D\,^2\Sigma^+)$	26.045	(9)
$N^+(^1D)+NO(A\,^2\Sigma^+)$	26.814	(10)
$N^+(^1D)+NO(B\,^2\Pi)$	27.057	(11)
$N^+(^1D)+NO(C\,^2\Sigma^+)$	27.829	(12)
$N^+(^1D)+N(^4S)+O(^3P)$	27.870	(13)
$N^+(^3P)+N(^4S)+O(^1D)$	27.938	(14)
$N^+(^1D)+NO(D\,^2\Sigma^+)$	27.945	(15)
$N^+(^3P)+N(^2D)+O(^3P)$	28.354	(16)
$N^+(^1S)+NO(A\,^2\Sigma^+)$	28.966	(17)
$N^+(^1S)+NO(B\,^2\Pi)$	29.209	(18)
$N^+(^3P)+N(^2P)+O(^3P)$	29.547	(19)
$N^+(^1D)+N(^4S)+O(^1D)$	29.837	(20)
$N^+(^1S)+NO(C\,^2\Sigma^+)$	29.981	(21)

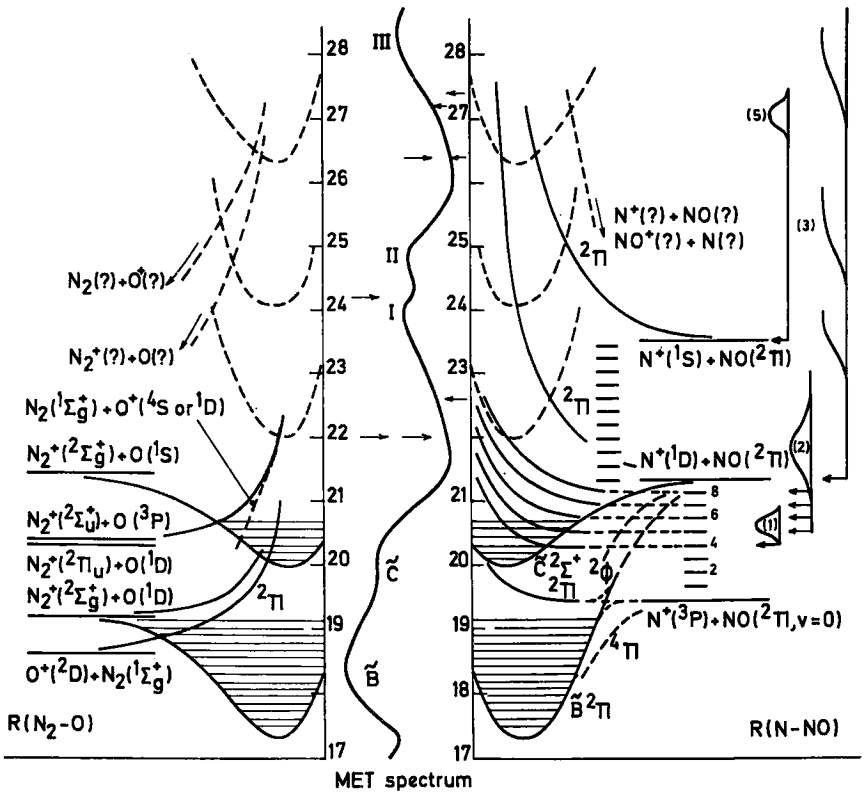

Fig. 11. Schematic potential energy diagram of N_2O along the two coordinates N–NO and N_2–O from 17 to 28 eV potential energy. The dipole (e, 2e) spectrum (MET) between 17 and 28 eV is inserted [16].

could play a role at 20.26 eV as shown in fig. 11.

A drastic change in slope at 20.9 eV points out the occurrence of a new N^+ producing mechanism. The straight line (2) extrapolates to 19.52 eV and is characterized by a slope of 0.29 (correlation coefficient $r = 0.993$). Appearance energies are measured from 21.6 up to 22.6 eV for kinetic energies of 0.5 to 0.9 eV carried by N^+.

The extrapolated energy of 19.52 eV is in good agreement with the dissociation energy of 19.46 calculated for process (1).

The slope of segment (2) indicates the partial conversion of the excess energy, with respect to 19.52 eV, into translational (40%) and vibrational (60%) energy. The energy balance made on each appearance energy shows $NO(X\,^2\Pi)$ to be formed

Table 5
Discrete values (meV) observed in the kinetic energy distribution of N^+/N_2O. Column 3 is the total energy calculated with respect to the first ionization energy of the N_2O^+ ($\tilde{C}\,^2\Sigma^+$) state [2]

KE (N^+)	Total KE	Total energy	PES [10]
0.0± 4	0	20.105	20.105 (0, 0, 0)
79 ± 7	116±10	20.221	20.223 (2, 2, 0)
155 ±15	227±20	20.332	20.388 (0, 0, 1)
220 ±15	322±20	20.427	20.538
275 ±15	375±20	20.475	20.538 (1, 0, 1)

in the vibrational levels $v = 5$ to 8. The N^+ appearance mechanisms should be

$$N_2O + e^- \rightarrow N_2O^{+*} \text{ or } N_2O^{**} \rightarrow NO(X\,^2\Pi, v = 5\text{–}8) + N^+(^4S),$$

where the intermediate state(s) is (are) unknown. However the "adiabatic" ionization energy of the first doubly excited state of N_2O^+ is ≈ 22.5 eV and can therefore be disregarded. It seems reasonable to suggest that in the energy range 20.9–22.6 eV, the N^+ ions appear through a direct transition to the repulsive surface $^2\Pi$ leading to $NO(X\,^2\Pi)$ in its vibrational levels $v = 5$ to 8. This situation is schematically drawn in fig. 11.

The straight line (3) in fig. 9 covers a wide kinetic energy range, i.e. 1.0–5.0 eV. The corresponding electron energy spreads over 22.6–28.5 eV. The least-squares fit, calculated on the nine first threshold energy measurements, gives a slope of 0.67 and an extrapolated energy of 21.27 eV for $KE(N^+) = 0.0$ eV with a correlation coefficient of 0.999.

The extrapolated energy of 21.27 eV would correspond to the thermodynamic onset of 21.36 eV calculated for process (2) in table 4. On the other hand the slope of 0.67, compared to the expected value of 0.68, unambiguously indicates that over the whole energy range considered, the excess energy with respect to 21.27 eV is converted into translational energy of the fragments.

The "break" in the kinetic energy versus appearance energy diagram is located at ≈ 22.6 eV. This energy has to be compared with the "adiabatic" ionization energy of the first doubly excited ionic N_2O^+ state (labelled I in table 3). The straight line (3) covers the energy range of both bands (I) and (II) of the dipole (e, 2e) spectrum of N_2O [16] inserted in fig. 11.

Quantum-mechanical calculations have been performed by Lorquet and Cadet [12] in this energy range. The combination of spectroscopic terms $NO(X\,^2\Pi)$ and $N^+(^1D)$, resulting from process (2) in table 4, gives rise to doublet Σ^+, Σ^-, Π [2], Δ and Φ states [12]. Furthermore the $\tilde{B}\,^2\Pi$, $\tilde{C}\,^2\Sigma^+$, $^2\Phi$ and a repulsive $^2\Pi$ states are shown to converge to 21.36 eV [12].

From the results of both the (e, 2e) spectrum and the present work, several ionic states of N_2O^+ (at least two) are dissociated to the same limit at 21.36 eV. The repulsive $^2\Pi$ state would be a candidate for predissociating these doubly excited ionic states and the proposed N^+ producing mechanism would be

$$N_2O + e^- \rightarrow N_2O^{+*}(22.6\text{–}28.5 \text{ eV}) + 2e^- \xrightarrow{\text{pred.}} NO(X\,^2\Pi, v = 0) + N^+(^1D) + KE.$$
$^2\Pi$

A second process occurs at the same dissociation limit, i.e. 21.36 eV [straight line (4) in fig. 9]. The slope of this segment is 0.24 and this value implies that $\approx 60\%$ of the excess energy involved in this process is converted into internal energy of the neutral fragment $NO(X\,^2\Pi)$. The segment (4) extends from 21.2 to 24.5 eV for kinetic energies ranging from 0.0 to 0.9 eV. The same mechanism as mentioned above, is expected for N^+ ion production, i.e.

$$N_2O + e^- \rightarrow N_2O^{+*}(I) + 2e^- \rightarrow NO(X\,^2\Pi, v = 0\text{–}10) + N^+(^1D),$$

where the $NO(X\,^2\Pi)$ molecule is produced in the vibrational energy levels $v = 0$–10.

Between 24.5 and 26.4 eV a broad energy gap is observed in the kinetic energy versus appearance energy diagram and a vertical line (5) rises up to 2.4 eV kinetic energy at an electron energy of 26.4 eV. This energy is close to the adiabatic ionization energy of the doubly excited state labelled (II) in table 3 with a vertical ionization energy of 28.5 eV [16].

At this level two interpretations of the vertical line are possible. First, the vertical line (5) could converge to segment (3). This means that the two last experimental onset energies on the straight line (3) are related to the decomposition of the doubly excited state (II) of N_2O^+ to the dissociation limit at 21.36 eV. This mechanism has already been suggested earlier in this discussion. The vertical line should only mean that no shift in onset energy is measured as long as the retarding potential is lower than or equal to the minimum kinetic energy of the N^+ ions. The upper experimental points pertaining to segment (5) could not be measured because of lack of energy resolution.

On the other hand, for higher retarding potentials, i.e. 2.8–3.5 eV, three onsets [segment (5′) in fig. 9] were measured, clearly deviating from the vertical line (5). These points could fit a straight line with a slope of 0.64 and extrapolating to ≈ 23.2 eV. This energy is close to the energy of 23.5 eV calculated for the onset of process (3) in table 4. This would mean that the doubly excited ionic state (II) has a second decomposition path way, i.e.

$$N_2O + e^- \rightarrow N_2O^+{}^*(II) + 2e^-$$
$$\xrightarrow[^2\Pi]{\text{pred.}} N^+(^1S) + NO(X\,^2\Pi, v = 0),$$

where the doubly excited state (II) has to be predissociated by a $^2\Pi$ state, the only one which is correlated with the spectroscopic terms $N^+(^1S)$ and $NO(X\,^2\Pi)$. The situation is schematically drawn in fig. 11.

At high electron energy, four vertical lines labelled (6)–(8) are drawn through the experimental points in fig. 9. They occur at the average energies of 27.4 ± 0.1 eV (6), 31.9 ± 0.16 eV (7), 37.3 ± 0.2 and 39.0 ± 0.1 eV (8) respectively. These vertical lines have to correspond to the decomposition of the doubly excited states of N_2O^+, the onsets covering the energy range of the doubly excited ionic states III–VI in table 3. Dissociation would occur via predissociation.

The absence of an inclined segment does not allow an identification of the dissociation limits involved in these processes.

Segment (6) however extends only over a 0–1.0 eV kinetic energy range. This means that the N^+ ions carry at least 1.0 eV translational energy. The absence of an inclined segment would be indicative of a narrow distribution centered at 1 eV. Taking this value together with the appearance energy of 27.4 eV, a simple energy balance would lead to a dissociation limit at 25.93 eV. This energy corresponds to processes (7)–(9) in table 4. However process (8) has to be discarded, involving three atomic fragments. This would imply that 1 eV kinetic energy carried by the N^+ ion, corresponds to 5.5 eV total translational energy involved in the dissociation process (8). The dissociation limit would lie at 21.9 eV, in drastic disagreement with the thermodynamical onset calculated for process (8).

Between 37.3 and 39.0 eV a singularity is to be noted: a negative slope for the linear dependence of the kinetic energy carried away by N^+ upon the ionizing electron energy. As far as we know, this is the first time that such a dependence is observed.

Due to the lack of any data on the shape of the potential energy surfaces of the doubly excited ionic states of N_2O^+, only ad hoc interpretations could account for this singular behaviour such as radiative deactivation of the excited state with emission of radiation or an energetic electron.

5. Conclusions

The present work is the second part of a dissociative electroionization study of N_2O^+. The channels producing O^+ and N^+ were examined and the discussion of the experimental results enabled us to conclude that predissociation is the main mechanism producing O^+ and N^+. In agreement with photon impact studies [2–5], the ground and excited states of N_2O^+ are involved. The present experiments extended the investigations to the doubly excited ionic states of N_2O^+ (see fig. 11).

In the O^+ producing channel, the predissociating state responsible for most of the fragmentation observed is the $N_2O^+(^4\Sigma^-)$ state. This state would even predissociate doubly excited states. Repulsive $N_2O^+(^2\Pi)$ states become important at higher energies. Furthermore, the present study shows the neutral fragment $N_2(X\,^1\Sigma_g^+)$ to be produced in vibrationally excited states.

In the N^+ producing channel, the predissociating states are $^2\Pi$ states which cross the $N_2O^+(\tilde{C}\,^2\Sigma^+)$ state and the doubly excited states of N_2O^+. As for N_2 formation, the neutral fragment $NO(X\,^2\Pi)$ is also mainly produced in vibrationally excited states.

Acknowledgement

We acknowledge the Fonds de la Recherche Fondamentale Collective (FRFC) and the Action

de Recherche Concertée (ARC) for financial support. One of us (JLO) is indebted to the ARC for a research grant.

References

[1] J.L. Olivier, R. Locht and J. Momigny, Chem. Phys. 68 (1982) 201.
[2] J. Berkowitz and J.H.D. Eland, J. Chem. Phys. 67 (1977) 2740.
[3] J.H.D. Eland, Intern. J. Mass Spectrom. Ion Phys. 12 (1973) 389;
B. Brehm, R. Frey, A. Kustler and J.H.D. Eland, Intern. J. Mass Spectrom. Ion Phys. 13 (1974) 257.
[4] T. Baer, P.M. Guyon, I. Nenner, A. Tabche-Fouhaille, R. Botter, L.F.A. Ferreira and T.R. Govers, J. Chem. Phys. 70 (1979) 1585.
[5] I. Nenner, P.M. Guyon, T. Baer and T.R. Govers, J. Chem. Phys. 72 (1980) 6587.
[6] R. Locht and J. Schopman, Intern. J. Mass Spectrom. Ion Phys. 15 (1974) 361.
[7] G. Herzberg, Molecular spectra and molecular structure, Vol. 3. Electronic spectra and electronic structure of polyatomic molecules (Van Nostrand, Princeton, 1967).
[8] G. Herzberg, Molecular spectra and molecular structure, Vol. 1. Spectra of diatomic molecules (Van Nostrand, Princeton, 1967).
[9] C.E. Moore, Atomic Energy Levels, Vol. 1, NBS Circular 467 (1949); Ionization Potentials and Ionization Limits derived from the Analysis of Optical Spectra, NSRDS-NBS34 (1970).
[10] P.M. Dehmer, J.L. Dehmer and W.A. Chupka, J. Chem. Phys. 73 (1980) 126.
[11] J. Schopman and R. Locht, Chem. Phys. Letters 26 (1974) 596.
[12] J.C. Lorquet and C. Cadet, Intern. J. Mass Spectrom. Ion Phys. 7 (1971) 245.
[13] R. Frey, B. Gotchev, W.B. Peatman, H. Pollak and E.W. Schlag, DESY Report SR-77/23.
[14] H. Köppel, L.S. Cederbaum and W. Domcke, Chem. Phys. 69 (1982) 175.
[15] A.W. Potts and T.A. Williams, J. Electron Spectry. 3 (1974) 3.
[16] C.E. Brion and K.H. Tan, Chem. Phys. 34 (1978) 141.
[17] W. Domcke, L.S. Cederbaum, J. Schirmer, W. von Niessen, C.E. Brion and K.H. Tan, Chem. Phys. 40 (1979) 171.
[18] U. Gelius, J. Electron Spectry. 5 (1974) 985.